Free Radical Biology and Medicine 99 (2016) 244–258

Contents lists available at ScienceDirect

Free Radical Biology and Medicine

journal homepage: www.elsevier.com/locate/freeradbiomed

Original article

DUX4-induced constitutive DNA damage and oxidative stress contribute to aberrant differentiation of myoblasts from FSHD patients

Petr Dmitriev [a,b,1], Yara Bou Saada [a,1], Carla Dib [a], Eugénie Ansseau [d], Ana Barat [a], Aline Hamade [e], Philippe Dessen [c], Thomas Robert [c], Vladimir Lazar [c], Ruy A.N. Louzada [g], Corinne Dupuy [g], Vlada Zakharova [f], Gilles Carnac [b], Marc Lipinski [a], Yegor S. Vassetzky [a,f,*]

[a] UMR 8126, Univ. Paris-Sud, CNRS, Institut de Cancérologie Gustave-Roussy, F-94805 Villejuif, France
[b] PhyMedExp, University of Montpellier, INSERM U1046, CNRS UMR 9214, F-34295 Montpellier cedex 5, France
[c] Functional Genomics Unit, Institut de Cancérologie Gustave-Roussy, F-94805 Villejuif, France
[d] Laboratory of Molecular Biology, University of Mons, 20 place du Parc, B700 Mons, Belgium
[e] ER030-EDST, Department of Life and Earth Sciences, Faculty of Sciences II, Lebanese University, Lebanon
[f] Lomonosov Moscow State University, Faculty of Bioengineering and Bioinformatics, 119991 Moscow, Russia
[g] UMR 8200, Univ., Paris-Sud, CNRS, Institut de Cancérologie Gustave-Roussy, F-94805 Villejuif, France

ARTICLE INFO

Article history:
Received 31 March 2016
Received in revised form
4 August 2016
Accepted 8 August 2016
Available online 9 August 2016

Keywords:
Facioscapulohumeral dystrophy
DNA damage
DUX4
Oxidative stress
Antioxidants

ABSTRACT

Facioscapulohumeral dystrophy (FSHD) is one of the three most common muscular dystrophies in the Western world, however, its etiology remains only partially understood. Here, we provide evidence of constitutive DNA damage in *in vitro* cultured myoblasts isolated from FSHD patients and demonstrate oxidative DNA damage implication in the differentiation of these cells into phenotypically-aberrant myotubes. Double homeobox 4 (DUX4), the major actor in FSHD pathology induced DNA damage accumulation when overexpressed in normal human myoblasts, and RNAi-mediated DUX4 inhibition reduced the level of DNA damage in FSHD myoblasts. Addition of tempol, a powerful antioxidant, to the culture medium of proliferating *DUX4*-transfected myoblasts and FSHD myoblasts reduced the level of DNA damage, suggesting that DNA alterations are mainly due to oxidative stress. Antioxidant treatment during the myogenic differentiation of FSHD myoblasts significantly reduced morphological defects in myotube formation. We propose that the induction of DNA damage is a novel function of the DUX4 protein affecting myogenic differentiation of FSHD myoblasts.

1. Introduction

Facioscapulohumeral dystrophy (FSHD) is an autosomal dominant disease manifesting mainly as wasting of specific groups of facial and limb muscles. The prevalence of FSHD is estimated to be as high as 8 in 100,000 suggesting that it might be the most common muscular dystrophy in the Western world [1]. FSHD has been genetically linked to a shortened macrosatellite repeat array D4Z4, specific polymorphisms and sequence variants on the long arm of chromosome 4 (region 4q35) which together are thought to create a context permissive for aberrant gene expression (reviewed in [2,3]).

Every D4Z4 repeat on chromosome 4q35 contains a promoter and a coding region for the *DUX4* gene. Several studies have documented a higher level of expression of *DUX4* as well as several proximally located genes in FSHD cells and tissues (reviewed in [2,3]). Transcriptomic and proteomic studies have revealed an abnormal expression of a number of mRNA, microRNAs and proteins in *in vitro* cultured myoblasts isolated from FSHD patients as compared to healthy controls [4–18].

In vitro cultured FSHD myoblasts which suffer from a defect in the myogenic differentiation program [5], demonstrate a low fusion index and morphological abnormalities when differentiated into myotubes [18,19] and are sensitive to oxidative stress [19,20]. In agreement with these observations, it was demonstrated that the expression of oxidative stress-related genes was altered in FSHD cells [7,8,11,12,20,21] and tissues [9,22] suggesting that FSHD cells might be subjected to an endogenous oxidative stress.

Increasing evidence indicates that oxidative stress can reduce the differentiation efficiency of human myoblasts; persistent reactive oxygen species (ROS) act as signaling molecules in several

* Corresponding author at: UMR 8200, Univ., Paris-Sud, CNRS, Institut de Cancérologie Gustave-Roussy, F-94805 Villejuif, France.
E-mail address: vassetzky@igr.fr (Y.S. Vassetzky).
[1] These authors contributed equally to this work.

http://dx.doi.org/10.1016/j.freeradbiomed.2016.08.007
0891-5849/

physiological processes in human skeletal muscle cells, they are notably known to affect their morphology and function (for review see [23,24]); both increased mitochondrial production of ROS and NF-kB signaling linked to increased production of ROS can lead to muscle atrophy [25,26].

Several previous observations suggest that increased *DUX4* expression might provoke oxidative stress. DUX4, when overexpressed in mouse immortalized myoblasts C2C12 or human rhabdomyosarcoma cell line RD, altered the expression of genes controlling redox balance and genes involved in the Nrf2-mediated oxidative stress response pathway [21,27]. Furthermore, inducible *DUX4* overexpression in C2C12 cells rendered them more sensitive to paraquat, a pro-oxidant compound [27]. However, the increased production of ROS in cells overexpressing *DUX4* has never been demonstrated directly.

Oxidative stress is known to induce toxic effects through production of peroxides and free radicals that damage proteins, lipids, and DNA in the cell. DNA damage and genetic instability are known to be involved in the etiology of many human diseases including cancer, neurodegenerative disorders, and aging (for review see [28,29]) and were also described in Duchenne (DMD) and Limb-girdle Muscular (LGMD) dystrophies, but not in FSHD [30] (for review see [31]).

Here we describe a novel phenotypic feature of *in vitro* cultured FSHD myoblasts: a high level of DNA damage lesions, increased production of ROS and upregulation of many genes related to DNA damage repair. Furthermore, we demonstrated for the first time that *DUX4* overexpression in human immortalized myoblasts results in a higher level of ROS in these cells. We also demonstrated that DNA damage and increased production of ROS were closely implicated in FSHD pathophysiology and that treatment of FSHD myoblasts with an antioxidant during myogenic differentiation significantly improved the phenotype of resulting FSHD myotubes.

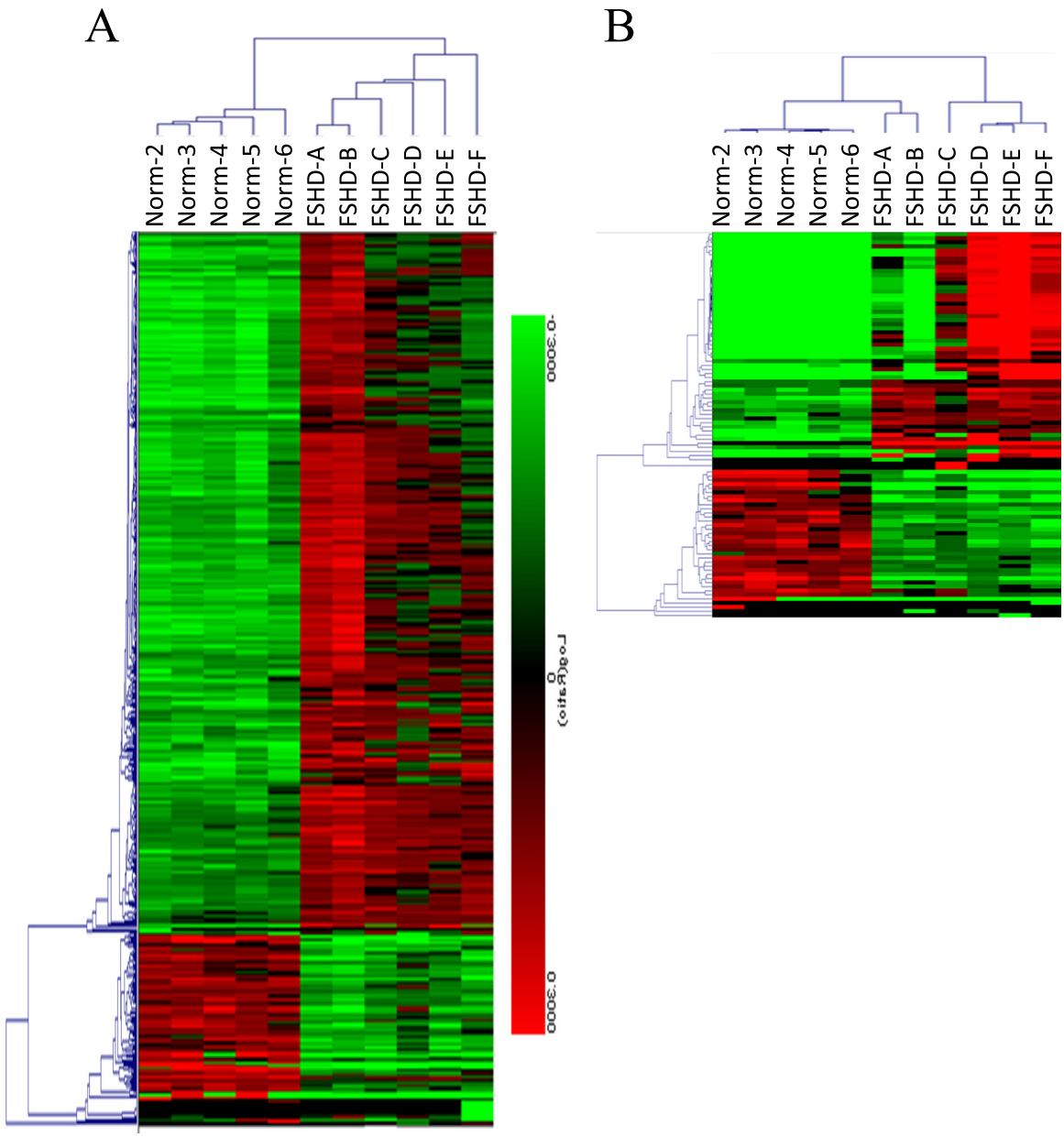

Fig. 1. Supervised clustering of gene expression profiles of *in vitro* cultured primary myoblasts (A) isolated from five healthy individuals (Norm-2,3,4,6) and six FSHD patients (FSHD-A,B,C,D,E,F) and myotubes derived from these myoblasts (B).

2. Results

2.1. Transcriptome profiling of FSHD myoblasts

Several transcriptome analyses of FSHD muscles have been carried out so far, but many of these studies were done either on biopsies or on non-purified myoblasts containing contaminating fibroblasts and adipocytes [7,10,12]. To gain insight into mechanisms of FSHD, we have analyzed transcriptional profiles in purified $CD56^{+}$ myoblasts and myotubes derived from either normal subjects or FSHD patients as described elsewhere [19]. Agilent Human Genome $8 \times 44K$ microarrays were used to identify differentially expressed genes as described in Materials and Methods. Microarray analysis of FSHD myoblasts revealed 312 up- and 88 downregulated protein-coding genes (Fig. 1**A**), while only 71 and 38 protein-coding genes were respectively up- and downregulated in FSHD myotubes (Fig. 1**B**) as compared to myoblasts and myotubes isolated from healthy subjects (Table 1**,** Supplementary Tables S1, S3–6).

The functional annotation of 312 genes upregulated in FSHD myoblasts resulted in 8 superclusters, each integrating several similar Gene Ontology (GO) functional categories (Supplementary Table S2); the three largest superclusters were *Regulation of cell cycle*, *DNA repair* and *Chromatin organization*. Interestingly, 29 genes upregulated in FSHD myoblasts were involved both in cell cycle regulation and DNA damage detection and repair. In total, 54 genes upregulated in proliferating FSHD myoblasts were involved in DNA damage repair (Table 2 **and** Supplementary Table S4).

Genes downregulated in FSHD myoblasts constituted a unique functional class, *Cell adhesion*; genes upregulated in FSHD myotubes produced a single marginally significant GO functional category, *Cell motility and migration*, while no significant functional category could be attributed to the genes downregulated in FSHD myotubes (Table 3 and Supplementary Table S5).

2.2. DNA damage in FSHD myoblasts

In order to substantiate the transcriptomic data, we tested the phosphorylation of histone H2A variant H2AX at Ser-139 (γH2AX), a marker for DNA damage that correlated with the presence of DNA double-stranded breaks (DSB). Using immunoblotting we found that the overall level of γH2AX in the protein extracts of FSHD myoblasts was significantly higher as compared to normal myoblasts (Fig. 2A and B). Immunofluorescent microscopy revealed a higher percentage of nuclei with γH2AX foci in FSHD myoblasts than in normal cells (Fig. 2C and D). The observation that a large number of DNA Damage Response (DDR)-related genes were upregulated in FSHD myoblasts and were accompanied by a significantly higher level of γH2AX foci as well as a higher level of the overall γH2AX prompted us to test the integrity of DNA in these cells. We quantified the number of apurinic/apyrimidinic (AP)-sites using ELISA. Single-stranded breaks (SSB) and DSB breaks were quantified using single-cell gel electrophoresis (comet assay) in alkaline conditions [32–34].

FSHD cells showed approximately 1.6 times more AP sites than normal myoblasts (Fig. 2E and Supplementary Fig. S1D), and the genomic DNA of normal cells contained significantly fewer breaks as compared to FSHD myoblasts, as shown by the analysis of the comet tail moment (TM) which reflects the degree of DNA damage (Fig. 3A, B and Supplementary Fig. S1A, B, C). In addition, the analysis of the TM distribution was distinct between FSHD and normal myoblasts; the TM of the majority of FSHD cells ranged

Table 1
Top-10 protein-coding genes differentially expressed in FSHD myoblasts (MB) and myotubes (MT) from 6 FSHD patients, as compared to those from 5 normal individuals. Members of the same gene family were omitted; FC - Fold change FSHD *vs.* normal samples.

MB upregulated			**MT upregulated**		
FC	**Gene name**	**Description:**	**FC**	**Gene name**	**Description:**
7.1	KCNA1	potassium channel, voltage gated shaker related subfamily A, member 1	79.2	RFPL2	ret finger protein-like 2
4.5	CALCR	calcitonin receptor	60.3	TRIM43	tripartite motif containing 43
3.4	ZYG11A	zyg-11 family member A, cell cycle regulator	48.1	PRAMEF1	PRAME family member 1
3.2	MPP4	membrane protein, palmitoylated 4 (MAGUK p55 subfamily member 4)	45.3	TRIM64	tripartite motif containing 64
2.8	COL13A1	collagen, type XIII, alpha 1	40.9	LEUTX	leucine twenty homeobox
2.8	PCDH9	protocadherin 9	30.2	SLC34A2	solute carrier family 34 (type II sodium/phosphate co-transporter), member 2
2.4	EPB41L4B	erythrocyte membrane protein band 4,1 like 4B	28.9	ZSCAN4	zinc finger and SCAN domain containing 4
2.4	ZNF367	zinc finger protein 367	25.7	KHDC1	KH homology domain containing 1
2.3	FAM111B	family with sequence similarity 111, member B	22.8	CCNA1	cyclin A1
2.3	TCF19	transcription factor 19	17.8	MBD3L3	methyl-CpG binding domain protein 3-like 3
303 more genes with FC > 1.2			**61 more gene with FC > 1.2**		
MB downregulated			**MT downregulated**		
FC	**Gene name**	**Description:**	**FC**	**Gene name**	**Description:**
−7.5	XAGE2	X antigen family, member 2	−16.6	PCDH10	protocadherin 10
−6.9	PCDH10	protocadherin 10	−7.3	AMPD1	adenosine monophosphate deaminase 1
−5.9	SEMA3E	sema domain, immunoglobulin domain (Ig), short basic domain, secreted, (semaphorin) 3E	−4.6	TP63	tumor protein p63
−5.3	CLSTN2	calsyntenin 2	−3.6	TRPA1	transient receptor potential cation channel, subfamily A, member 1
−4.8	DGKB	diacylglycerol kinase, beta 90 kDa	−3.1	PIEZO2	piezo-type mechanosensitive ion channel component 2
−4.4	PGM5	phosphoglucomutase 5	−3.0	RAET1E	retinoic acid early transcript 1E
−4.2	GRIP2	glutamate receptor interacting protein 2	−2.7	BCAS1	breast carcinoma amplified sequence 1
−3.5	APOE	apolipoprotein E	−2.2	TXLNB	taxilin beta
−3.2	VNN1	vanin 1	−2.2	LMOD3	leiomodin 3 (fetal)
−3.2	PRKG1	protein kinase. cGMP-dependent, type I	−2.0	LSMEM2	leucine-rich single-pass membrane protein 2
78 more genes with FC < −1.2			**28 more genes with FC < −1.2**		

Table 2
Functional classification of the 54 DNA damage-related genes differentially expressed in FSHD.

Gene name	Cell_cycle	DNA_Replication	DNA_repair	Chromatin_organization	Chromosome_segregation	Cytoskeleton	Meiosis	Cell_signaling	FC	Description
BLM	X	X	X	X					1.9	Bloom syndrome, RecQ helicase-like
BRCA1	X	X	X		X	X			1.7	breast cancer 1, early onset
BRCA2	X	X	X	X		X	X		1.9	breast cancer 2, early onset
CDC25C	X	X	X						1.9	cell division cycle 25 C
CDC6	X	X	X						1.9	cell division cycle 6
CDK2	X	X	X						1.8	cyclin-dependent kinase 2
CDT1	X	X	X						2.1	chromatin licensing and DNA replication factor 1
CENPF	X	X	X	X	X				1.9	centromere protein F, 350/400 kDa
CHAF1A	X	X	X	X					1.6	chromatin assembly factor 1, subunit A (p150)
CHAF1B	X	X	X	X					2.2	chromatin assembly factor 1, subunit B (p60)
CLSPN	X	X	X						2.1	claspin
DBF4	X	X	X						1.6	DBF4 zinc finger
DSCC1	X	X	X	X	X				1.9	defective in sister chromatid cohesion 1 homolog (S. cerevisiae)
DTL		X	X						2.1	denticleless E3 ubiquitin protein ligase homolog (Drosophila)
ESCO2	X		X						2.0	establishment of sister chromatid cohesion N-acetyltransferase 2
EXO1	X		X				X		1.8	exonuclease 1
FANCC			X						1.4	Fanconi anemia, complementation group C
FANCD2	X		X	X			X		2.0	Fanconi anemia, complementation group D2
FANCI	X		X						1.7	Fanconi anemia, complementation group I
FEN1		X	X					X	1.6	flap structure-specific endonuclease 1
H2AFX	X		X	X			X		1.6	H2A histone family, member X
HELLS	X		X	X					1.9	helicase, lymphoid-specific
HMGB1		X	X	X					1.5	high mobility group box 1
KIF22	X		X			X			1.6	kinesin family member 22
LIN9	X	X	X						1.7	lin-9 DREAM MuvB core complex component
MCM10		X	X						2.1	minichromosome maintenance complex component 10
MCM2	X	X	X	X					1.7	minichromosome maintenance complex component 2
MCM3	X	X	X						1.8	minichromosome maintenance complex component 3
MCM5	X	X	X						1.8	minichromosome maintenance complex component 5
MND1	X		X				X		1.9	meiotic nuclear divisions 1 homolog (S. cerevisiae)
MSH2	X		X	X					1.6	mutS homolog 2
NEIL3			X						2.2	nei endonuclease VIII-like 3 (E. coli)
PCNA		X	X					X	1.6	proliferating cell nuclear antigen
POLD3		X	X						1.6	polymerase (DNA-directed), delta 3, accessory subunit
POLE2		X	X						2.1	polymerase (DNA directed), epsilon 2, accessory subunit
POLQ		X	X						2.2	polymerase (DNA directed), theta
PRIM1		X	X						2.2	primase, DNA, polypeptide 1 (49 kDa)
PSIP1			X						1.9	PC4 and SFRS1 interacting protein 1
RAD51	X	X	X				X		1.8	RAD51 recombinase
RAD51AP1			X						1.9	RAD51 associated protein 1
RECQL4			X						1.5	RecQ protein-like 4
RFC2		X	X						1.7	replication factor C (activator 1) 2, 40 kDa
RFC4		X	X					X	1.7	replication factor C (activator 1) 4, 37 kDa
RFC5		X	X						2.0	replication factor C (activator 1) 5, 36.5 kDa
RNASEH2A		X	X						1.7	ribonuclease H2, subunit A
RPA1	X	X	X	X			X		1.4	replication protein A1, 70 kDa
RRM1		X	X						1.5	ribonucleotide reductase M1
RRM2		X	X						2.2	ribonucleotide reductase M2
TIPIN	X	X	X						1.6	TIMELESS interacting protein
TK1		X	X						1.7	thymidine kinase 1, soluble
TOP2A		X	X	X	X			X	1.8	topoisomerase (DNA) II alpha 170 kDa
TYMS		X	X					X	1.9	thymidylate *syn*thetase
USP1			X						1.5	ubiquitin specific peptidase 1
WRAP53			X	X					1.5	WD repeat containing, antisense to TP53

Table 3
Functional classification of genes differentially expressed in FSHD. MB, Myoblasts, MT Myotubes, FDR False discovery rate. P-value and FDR of a supercluster (Supplementary Table S2) correspond to those of the most significant GO function within it.

MB upregulated	**No of genes**	**p-value**	**FDR**
Unique protein-coding genes (FC > 1.2)	313		
Genes with a known function indexed in GO	266		
Best values for a random list	**266**	**1.60E-04**	**2.70E-01**
Functional supercluster			
Cell_cycle	109	4.50E-72	7.30E-69
DNA_Replication_and_nucleotide_biosynthesis	38	1.00E-29	1.60E-26
DNA_repair	54	1.40E-28	2.20E-25
Chromosome_and_chromatin_organization	68	1.60E-28	2.50E-25
Chromosome_segregation	26	9.80E-26	1.60E-22
Microtubule_cytoskeleton_organization and localization	34	8.20E-20	1.30E-16
Meiosis	14	5.90E-09	9.50E-06
Cell_signaling	18	1.70E-07	2.70E-04
Total unique genes	170		
MB downregulated	**No of genes**	**p-value**	**FDR**
Unique protein-coding genes(FC < −1.2)	88		
Genes with a known function indexed in GO	75		
Best values for a random list	**75**	**4.50E-03**	**6.60E+00**
Significant functional category (DAVID)			
none			
MT upregulated	**No of genes**	**p-value**	**FDR**
Unique protein-coding genes(FC > 1.2)	71		
Genes with a known function indexed in GO	52		
Best values for a random list	**52**	**9.80E-03**	**1.40E+01**
Significant functional category (DAVID)			
GO:0016477~cell migration	4	9.70E-03	9.9E-1
MT downregulated	**No of genes**	**p-value**	**FDR**
Unique protein-coding genes(FC < −1.2)	38		
Genes with a known function indexed in GO	27		
Best values for a random list	**27**	**6.70E-03**	**8.90E+00**
Significant functional category (DAVID)			
none			

between 100 and 150 (a.u.), whereas the TM of the majority of normal cells varied between 40 and 100 (a.u.) (Fig. 3C and Supplementary Fig. S1).

Cellular responses to DNA damage may induce cell cycle arrest. We next followed the cell cycle progression of several cultures of primary FSHD and normal myoblasts using BrdU labeling. The analysis of FACS data did not reveal any statistically significant deviation of the cell cycle distribution between FSHD and normal cells (Supplementary Figure S2). This result was in agreement with previous reports [35–37] and our own observations that *in vitro* cultured FSHD cells proliferated similarly to normal controls.

Taken together, our data clearly demonstrate higher levels of DNA damage in the FSHD myoblasts, although the extent of this damage was insufficient for cell cycle arrest.

2.3. *DUX4 induces DNA damage in FSHD*

In vitro overexpression of human *DUX4* gene in *in vitro* cultured mouse and human myogenic progenitor cells has been shown to interfere with their myogenic differentiation and to increase sensitivity to oxidative stress [27] thus reproducing some features of cultured FSHD myoblasts. In addition, overexpression of the human *DUX4* gene caused atrophy [38] and apoptosis [39] in human cells cultured *in vitro* and was deleterious for mouse and zebrafish muscles *in vivo* [40,41]. Together with the observation that RNAi-mediated *DUX4* inhibition was sufficient to reverse morphological abnormalities found in cultured FSHD myotubes [38], these findings suggest that *DUX4* overexpression may be one of the causes of FSHD.

To address the possibility that DUX4 might be also responsible for higher levels of DNA damage observed in FSHD cells, we overexpressed *DUX4* in human immortalized myoblasts and found that the level of DNA damage measured by the comet assay was 1.5 times higher in *DUX4*-overexpressing cells (Fig. 4**A**, **B**, **C** and Supplementary Figure S3). Similarly, the number of AP sites was two times higher in *DUX4*-overexpressing myoblasts as compared to the control cells (Fig. 4**D**). Furthermore, the analysis of γH2AX and DUX4 co-localization by immunofluorescence revealed that these two proteins were co-localized in 75% of *DUX4*-transfected cells *versus* 35% of *GFP*-transfected cells (Fig. 4**E**), and the overall level of γH2AX phosphorylation was higher in *DUX4*-overexpressing cells as compared to the control cells (Fig. 4**F** and **G**).

We then transfected primary myoblasts isolated from FSHD patients with siRNA against DUX4 and found that the *DUX4* knockdown diminished the level of DNA damage in FSHD myoblasts (Fig. 5). Taken together, our results demonstrate that the induction of DNA damage might be a novel FSHD-related function of DUX4.

FSHD cells are highly sensitive to oxidative stress [19,20,27]. However, a direct role of *DUX4* in the induction of oxidative stress has never been demonstrated. In order to determine the role of DUX4 in ROS generation, we have overexpressed *DUX4* in human immortalized myoblasts and measured the level of ROS using the dihydroethidium (DHE), a ROS fluorescent sensor probe that, once oxidized in the presence of cellular oxidants, exhibits a red fluorescence. We observed that the level of ROS was increased in *DUX4*-overexpressing myoblasts as compared to the controls (Fig. 6**A, C** and Supplementary Figure S4A). Furthermore, we confirmed this result by a complementary sensitive approach that uses Amplex Red probe (10-acetyl-3,7-dihydroxyphenoxazine) to detect H_2O_2

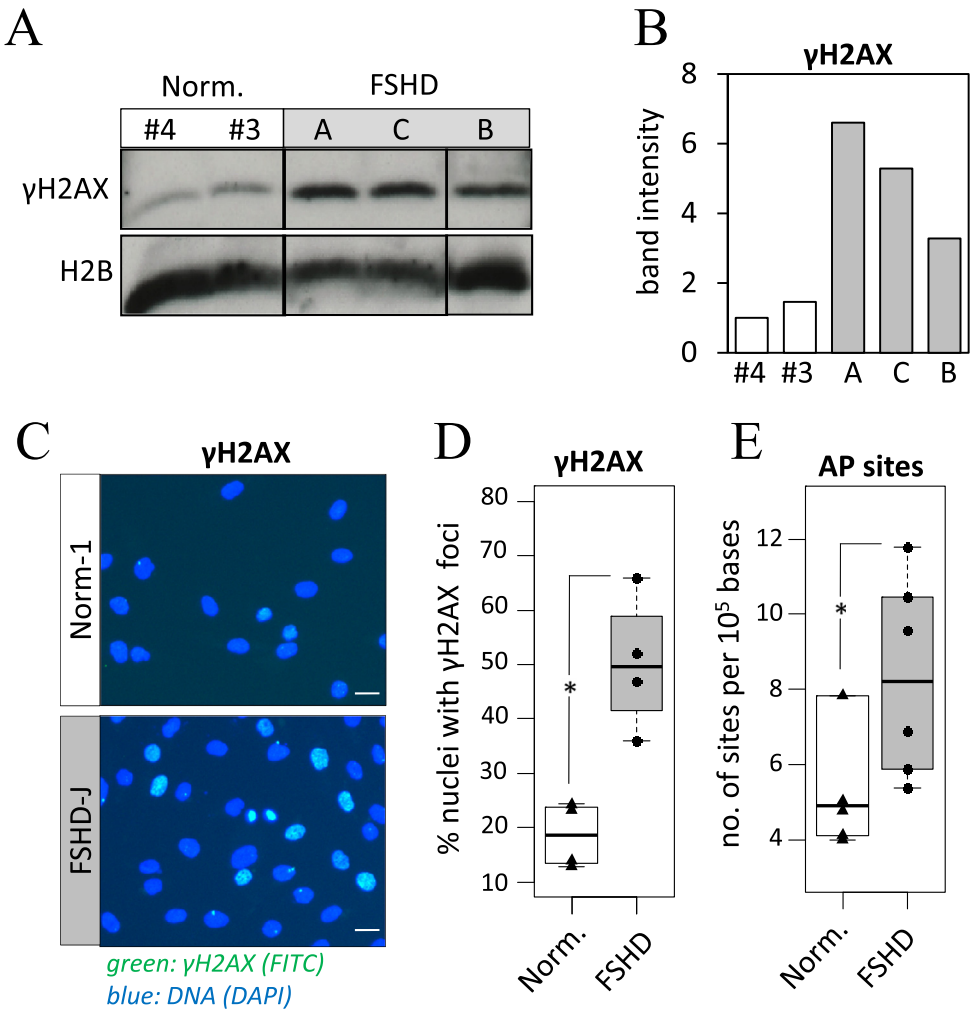

Fig. 2. DNA damage markers in FSHD myoblasts. **A.** Western blot analysis of γH2AX protein levels in FSHD primary myoblasts from FSHD patients (FSHD-A,B,C) and healthy controls (Norm-3,4). **B**. Densitometry quantification of the western blot images shown in panel A, γH2AX was normalized to H2B protein levels. **C**. Immunofluorescent imaging of γH2AX foci labeled with Alexa 488 in primary myoblasts from the FSHD patient FSHD-J and a healthy subject Norm-1; representative images are shown; 20X magnification, bar = 10 μm. **D**. Quantification of nuclei of primary myoblasts from four healthy subjects Norm-1,3,6,5 (triangles) and four FSHD patients FSHD-E,G,H,J (dots) containing γH2AX foci. Each dot/triangle in the boxplot represents the percentage of γH2AX foci in one cell culture, calculated from at least 100 nuclei. (*) - *t*-test p-value < 0.05. For given sample size and type I error rate alpha = 5%, power = 0.95. **E**. Average number of apurinic/apyrimidinic (AP) sites in primary myoblasts from six FSHD patients (FSHD-A,B,C,D,E,F) and five healthy controls (Norm-2,3,4,5,6); (*) *t*-test p-value < 0.05.

released to the extracellular space (Supplementary Figure S5) [42].

We hypothesized that the increased production of ROS in *DUX4*-overexpressing cells was a direct cause of DNA damage; therefore we treated *DUX4*-transfected cells with tempol, a potent antioxidant, and found that in the presence of tempol, the level of ROS significantly decreased (Fig. 6**A, B, C** and Supplementary Figure S4B, C) and the amount of DNA lesions was similar in *DUX4*-transfected cells as in mock-transfected and *GFP*-transfected cells (Fig. 4**A, B, C** and Supplementary Figure S3). This result indicates that the mechanism of DNA damage induced by DUX4, involves increased production of ROS in the cell.

2.4. DNA damage in FSHD myoblasts is provoked by ROS

Despite a number of studies, the oxidative stress has never been directly demonstrated in *in vitro* cultured FSHD cells. By measuring DHE fluorescence, we found that the level of ROS was considerably higher in *in vitro* cultured FSHD myoblasts as compared to normal controls (Fig. 6**D, E, F** and Supplementary Figure S6).

We then asked whether the DNA damage observed in *in vitro* cultured primary myoblasts from FSHD patients could be linked to oxidative stress. Thus we treated the FSHD myoblasts with tempol and quantified the level of DNA damage using comet assay. Our data clearly indicate that antioxidant-treated FSHD cells have a level of DNA damage indistinguishable from normal cells (Fig. 7). We concluded that the high level of DNA damage observed in FSHD myoblasts is provoked by higher levels of ROS.

2.5. DNA damage and ROS affect myogenic differentiation of FSHD myoblasts

In vitro cultured FSHD myoblasts give rise to abnormal myotubes upon myogenic differentiation induced by serum starvation [19]. These defects in differentiation could be due, at least partly, to overexpression of *DUX4* [38]. DNA damage and ROS can interfere with signal transduction pathways as they can act as second messengers for various physiological stimuli [43] and can thereby affect myotube formation and have pathological implications.

We have selected a primary FSHD culture, FSHD-F, known to differentiate into atrophic myotubes [18,19]. We treated proliferating myoblasts with 100 μM antioxidant tempol and 48 h post-treatment induced myogenic differentiation by serum starvation in the presence of tempol. Six days post-differentiation,

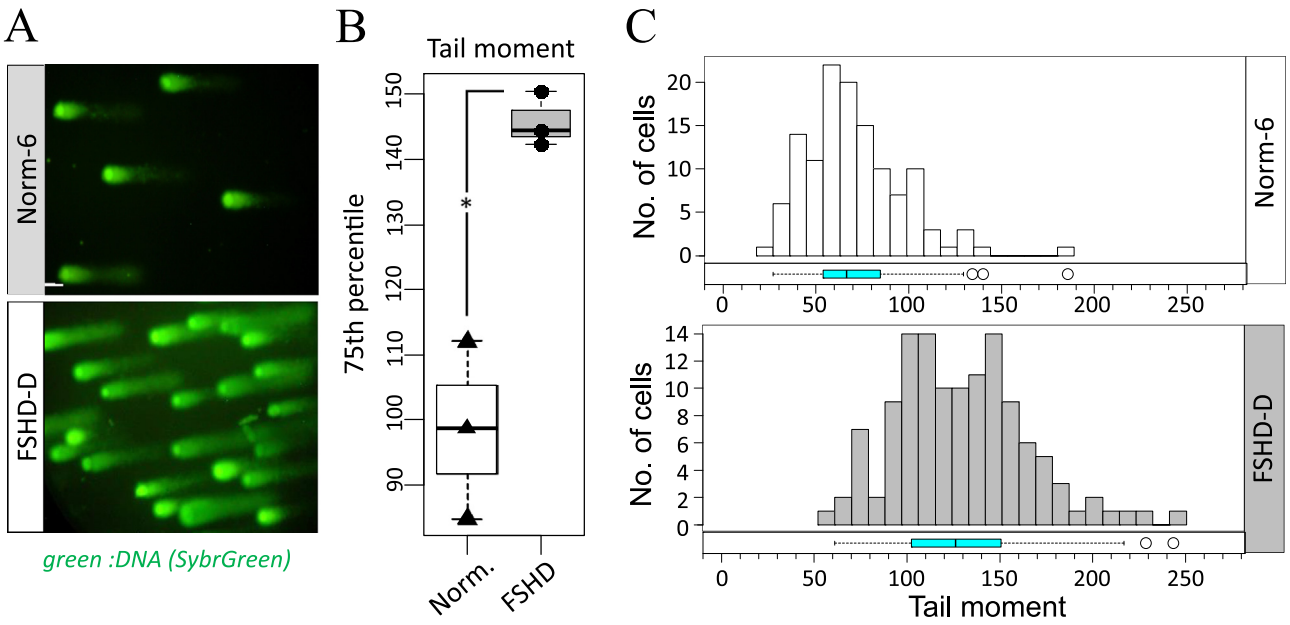

Fig. 3. DNA damage in FSHD myoblasts. **A**. Fluorescent imaging of primary myoblasts isolated from the FSHD patient FSHD-D and a healthy subject Norm-6 subjected to a single-cell electrophoresis (comet assay) and stained with SybrGreen; representative images are shown, 20X magnification, bar = 10 μm; **B**. 75th percentiles of comet tail moment distributions measured in primary myoblasts from three FSHD patients (FSHD-D,E,F) and three healthy controls (Norm-4,5,6), for each primary myoblast culture, at least 100 cells were analyzed; (*) *t*-test p-value < 0.05. For given sample size and type I error rate alpha = 5%, power = 0.989. **C**. Histogram and horizontally oriented boxplot showing the distribution of comet tail moments measured in primary myoblasts from patient FSHD-D (124 cells analyzed) and a healthy subject Norm-6 (125 cells analyzed); Distributions for other lines analyzed are shown in Supplementary Fig. S1.

non-treated FSHD-F myotubes were thin and atrophic, with a mean diameter of 11.7 μm. In the presence of tempol, the number of myotubes with larger diameter significantly increased and diameter reached a mean value of 15.1 μm (Fig. 8). We then tested another powerful antioxidant, N-Acetyl-L-cysteine (NAC), on FSHD-F myoblasts. NAC is a derivative of L-cysteine; its antioxidant activity is due to its ability to interact with the electrophilic groups of free radicals due to the presence of free thiol groups [44]. NAC was highly efficient and the diameter of NAC-treated FSHD-F myotubes (mean value of 21.3 μm) was closer to that of normal Norm-7 myotubes (mean value of 26.2 μm). These results suggest that oxidative stress affects myogenic differentiation process of FSHD myoblasts; it specifically contributes to establishment of phenotypically aberrant myotubes. The antioxidant treatment significantly improved the phenotype of FSHD myotubes.

3. Discussion

Here we performed a transcriptome profiling of $CD56^+$ FSHD myoblasts cultured *in vitro* by including a step of specific enrichment for myogenic cells and, thus avoided working on complex cell mixtures containing inflammatory-, connective tissue-, adipose tissue- and other cells; this excluded possible artifacts potentially introduced by the external factors such as inflammatory cells infiltrating FSHD muscles [45]. Previously, transcriptome and proteome profiling of FSHD biopsies and myoblasts demonstrated an abnormal expression of myogenesis-related mRNA and miRNAs [4–7,12,17]; cytoskeleton proteins [15]; genes related to oxidative stress [8,11,12,20]; vascular smooth muscle and endothelium cell-specific genes [9]; germline-related genes [13,14], genes specific to immune system [10] and others. Furthermore, abnormal expression of cell cycle-related genes has been documented using *in vitro* cultured FSHD myoblasts [11] and FSHD tissue samples [46]. In agreement with previous reports, we have found genes related to cytoskeleton (*i.e.* DIAPH3, PSRC1, TACC3) and oxidative stress (*i.e.* APOE, TRPA1, VNN1). Our transcriptome analysis also revealed an upregulation of many genes related to DNA damage repair in FSHD myoblasts. The probability of finding this group of genes linked by the common function by chance was very low (p-value = 1.4×10^{28}) and suggested the presence of a higher level of DNA damage in FSHD cells which was not previously observed. Here, by means of several techniques, we have demonstrated constitutive DNA damage in FSHD myoblasts.

Major DNA lesions include single-stranded DNA breaks (SSBs), double-stranded DNA breaks (DSBs) and abasic sites (AP-sites); they may be caused by external factors such as ionizing radiation, xenobiotic chemicals, UV, etc [47,48] and endogenous sources such as cellular metabolism [49], replicative stress and replicative fork collapse [50].

Since *in vitro* cell culture conditions excluded that the increased DNA damage in FSHD cells was due to external genotoxic factors, we focused on internal sources of DNA damage. At first, we ruled out the possibility that the DNA damage observed in FSHD cells was due to the replicative stress since in our experimental conditions, FSHD myoblasts were cycling normally and no difference in cell cycle progression was observed.

Another major internal cause of genomic DNA damage is cellular metabolism (for review see [28]) that routinely produces free radicals (ROS) reacting with the purine and pyrimidine bases and phosphate backbone of DNA.

As mentioned above, *in vitro* cultured myoblasts isolated from FSHD patients are sensitive to oxidative stress inducers Paraquat and H_2O_2 [19,20]. Coupled with the observation that the expression and biological activity of enzymes controlling the redox balance is altered in FSHD patients [22] these reports suggested that FSHD myoblasts might suffer from the endogenous oxidative stress, however, this has never been directly demonstrated before. Here, using fluorescent reactive oxygen species (ROS) sensor DHE, we could demonstrate that FSHD myoblasts contain higher level of ROS as compared to normal cells thus confirming the presence of oxidative stress in FSHD myoblasts *in vitro*. The DHE results were confirmed by Amplex Red data.

We then focused on the possibility that ROS was the major

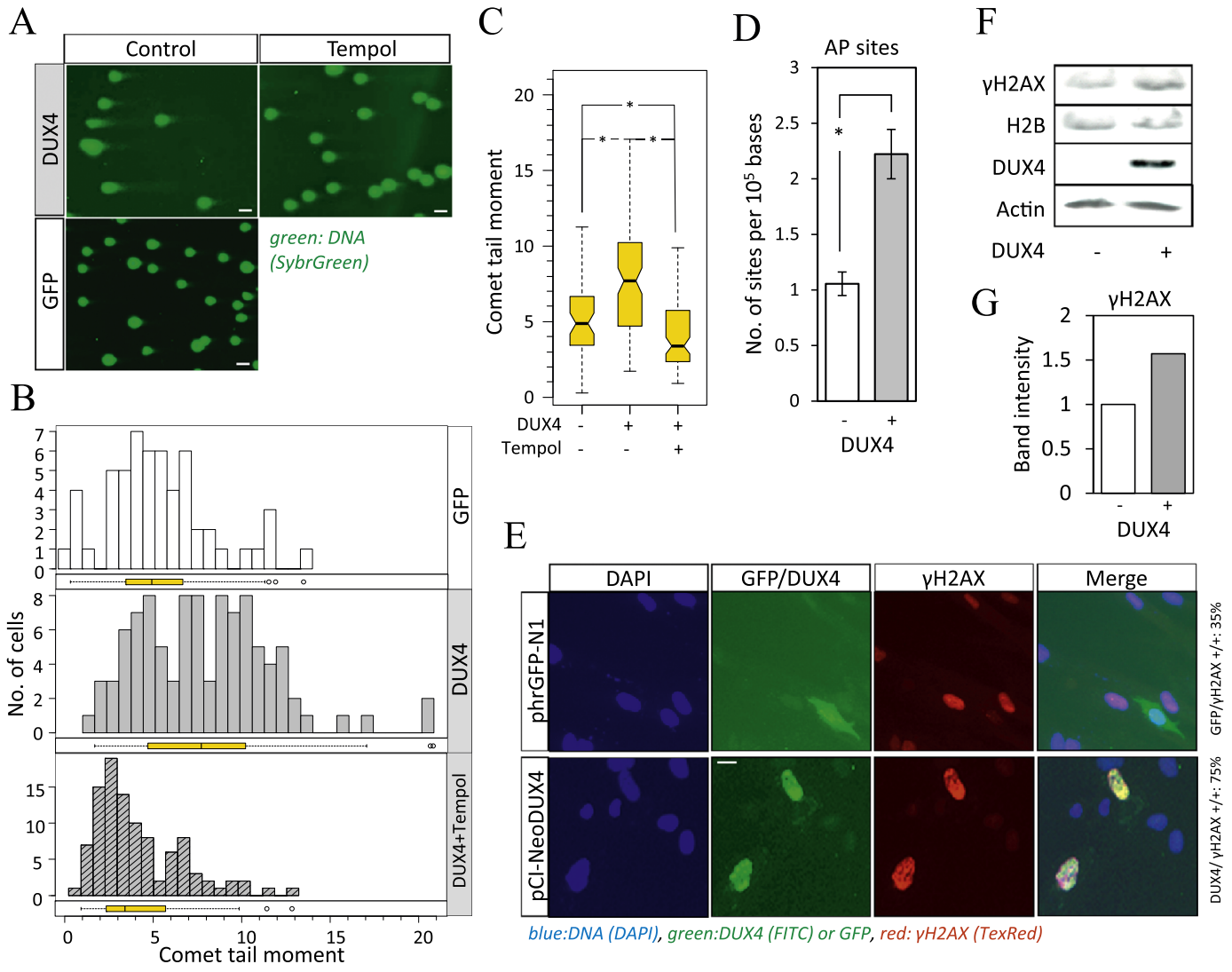

Fig. 4. DUX4-induced DNA damage in human myoblasts. **A.** Fluorescent imaging of DNA of human immortalized myoblasts transfected with pCI-Neo-DUX4 or control plasmid phrGFP-N1, treated or not with tempol and subjected to single cell alkaline gel electrophoresis (Comet assay), representative images at 20X magnification are shown, bar = 10 μm. **B.** Effect of tempol on the distribution of comet tail moments of immortalized myoblasts transfected with *DUX4* plasmid. At least 100 cells were analyzed per condition. **C.** Statistical analysis of comet tail moment distributions of human immortalized myoblasts transfected with *DUX4* or a control plasmid and treated or not with tempol. Results are obtained from 3 different experiments. (*) *t*-test p-value < 0.05. Notches indicate a confidence interval. **D.** Quantification of AP sites present in the DNA of rhabdomyosarcoma cells transfected with a *DUX4* or *GFP* plasmid. Results are obtained from 3 different experiments; (*) *t*-test p-value = 0.000176. **E.** Immunofluorescent imaging of human immortalized myoblasts transfected with pcI-Neo-DUX4 or phrGFP-N1 plasmid stained with antibodies against DUX4 and γH2AX; % of cells co-expressing *DUX4* and *γH2AX* or *GFP* and *γH2AX* and representative images at 20X magnification are shown, bar = 10 μm. **F.** Western blot analysis of *γH2AX* expression in rhabdomyosarcoma cells transfected with *DUX4* or *GFP* plasmid for 20 h. **G.** Densitometry quantification of the western blot images shown in **F**.

perpetrator in the development of a high level of damaged DNA in FSHD cells. The most stable product of oxidative modification of DNA is 8-hydroxy-2′-deoxyguanosine (8-OHdG) or its tautomer 8-oxo-7,8-dihydro-2-deoxyguanosine (8-oxoG) (for review see [51]) which is excised by DNA glycosylases resulting in the creation of an AP-site. The AP-site is thereafter converted to a SSB which might eventually result in a DSB [52] (for review see [53]). The treatment of FSHD myoblasts with tempol, a powerful antioxidant, efficiently reduced the level of DNA breaks in FSHD myoblasts. Taken together, our results provide evidence that oxidative stress is the source of DNA damage observed in FSHD myoblasts cultured *in vitro*.

We next elucidated the mechanism leading to the onset of oxidative stress and DNA damage in FSHD cells. It has been previously observed that the overexpression of human *DUX4* gene in mouse immortalized myoblasts C2C12 altered the expression of genes controlling red-ox balance and increased the sensitivity of the cells to Paraquat [27]. However, the direct role of DUX4 in the induction of oxidative stress has never been demonstrated. Here, for the first time we directly tested the level of ROS in *DUX4*-transfected cells and found that *DUX4* overexpression considerably increased the ROS level in the cells. Furthermore, we found that *DUX4* overexpression induced DNA damage in normal cells while *DUX4* knockdown diminished the level of damaged DNA in FSHD myoblasts suggesting that elevated *DUX4* expression in FSHD might be responsible for the constitutional DNA damage observed in these cells.

DUX4 might induce DNA damage in several ways: DUX4 is known to control the expression of genes involved in the establishment of the red-ox balance in the cell [21,27]. Consequently, by altering the oxidative metabolism, *DUX4* overexpression might directly or indirectly induce DNA damage in FSHD cells. Indeed, addition of an antioxidant into the culture medium of *DUX4*-overexpressing cells completely reversed the effect of DNA damage induced by the overexpression of *DUX4*. Our results indicate that the mechanism of DUX4-dependent DNA damage is related to ROS production. Induction of DNA damage is a novel function of

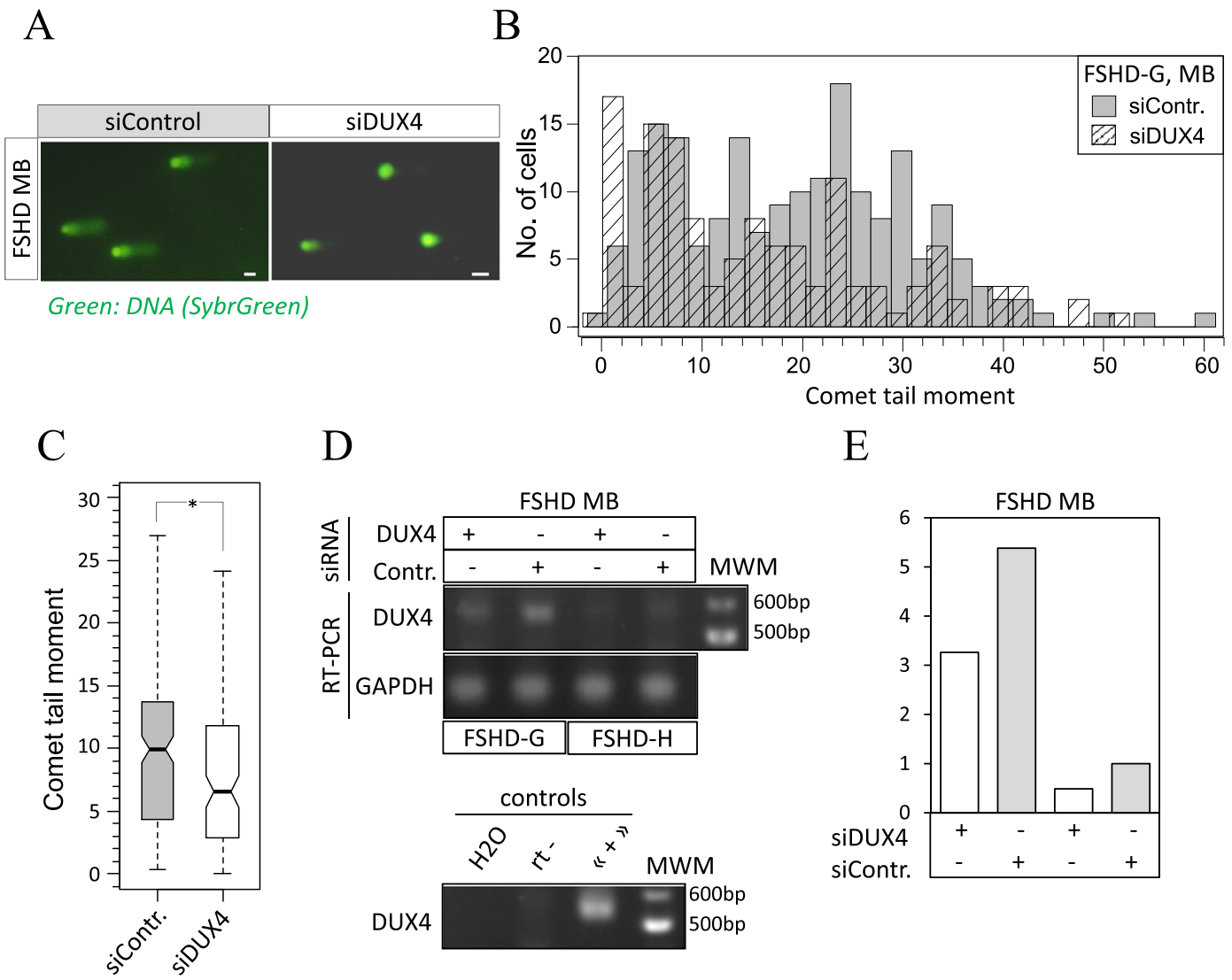

Fig. 5. Effect of *DUX4* knockdown on constitutive DNA damage in FSHD myoblasts. **A.** Fluorescent imaging of genomic DNA of FSHD myoblasts (FSHD-G) transfected with siRNA against DUX4 (siDUX4) or a control siRNA (siContr) and subjected to a single-cell gel electrophoresis in alkaline conditions, representative images with 10X magnification are shown, bar = 10 μm. **B.** Effect of *DUX4* knockdown on comet tail moment distribution for primary myoblasts from FSHD patient FSHD-G. 127 cells were analyzed for the "FSHD-G-siDUX4" condition and 193 cells - for "FSHD-G-siControl" condition. **C**. Statistical analysis of comet tail moment distributions shown in **B**; (*) *t*-test p-value < 0.05. **D.** *DUX4* expression in primary myoblasts isolated from two FSHD patients (FSHD-G and FSHD-H) and transfected with siRNA against DUX4 (siDUX4) or a control siRNA (siContr). RT-PCR products were separated on agarose gel and stained with EtBr. Below: RT-PCR controls: "+" - mouse C2C12 myoblasts transfected with a plasmid encoding two human D4Z4 elements encoding DUX4 under control of its natural promoter; "rt-" - no reverse transcriptase added to the reaction. "H_2O" - no template added to the reaction. MWM - molecular weight marker. **E**. Densitometry quantification of RT-PCR images from FSHD-G and FSHD-H shown in D.

DUX4 related to FSHD.

Genotoxic stress has been shown to interfere with normal myogenic differentiation (for review see [54]. Myoblasts carrying unrepaired DNA damage avoid formation of skeletal myofibers by prioritizing DNA repair over the activation of the myogenic program [55]. We then focused on the pathological implication of DNA damage and increased production of ROS on phenotype of FSHD myotubes and discovered that treatment of FSHD myoblasts with tempol during the myogenic differentiation process can significantly improve the phenotype of resulting myotubes. We also treated FSHD myoblasts with NAC which was previously used in dystrophin-deficient (mdx) mice to reduce myonecrosis and the level of inflammation in blood [56], and successfully helped to reduce the level of oxidized glutathione and oxidized thiol proteins in dystrophic muscles [57]. NAC-treated myotubes showed a larger diameter and a closer morphology to normal myotubes. Thus DNA damage and oxidative stress contribute to establishment of phenotypically- aberrant myotubes and the antioxidant treatment can improve the phenotype of FSHD myotubes.

The results of this work thus establish DNA damage as a novel phenotypic feature of FSHD cells which is dependent on *DUX4* expression. DNA damage and oxidative stress are implicated in the aberrant phenotype of *in vitro* FSHD myotubes and might be involved in a functional deviation of FSHD myoblasts from their normal counterparts.

4. Materials and methods

4.1. Cell culture conditions and transfection

Primary myoblasts ("pMyo") isolated from skeletal muscle biopsies of FSHD patients and healthy subjects (**Table S2**) and purified using CD56/NCAM magnetic beads (Miltenyui Biotec) as previously described [19] were obtained from Dr. Dalila Laoudj-Chenivesse (INSERM U-1046, Montpellier, France). They were cultured for up to 5 passages

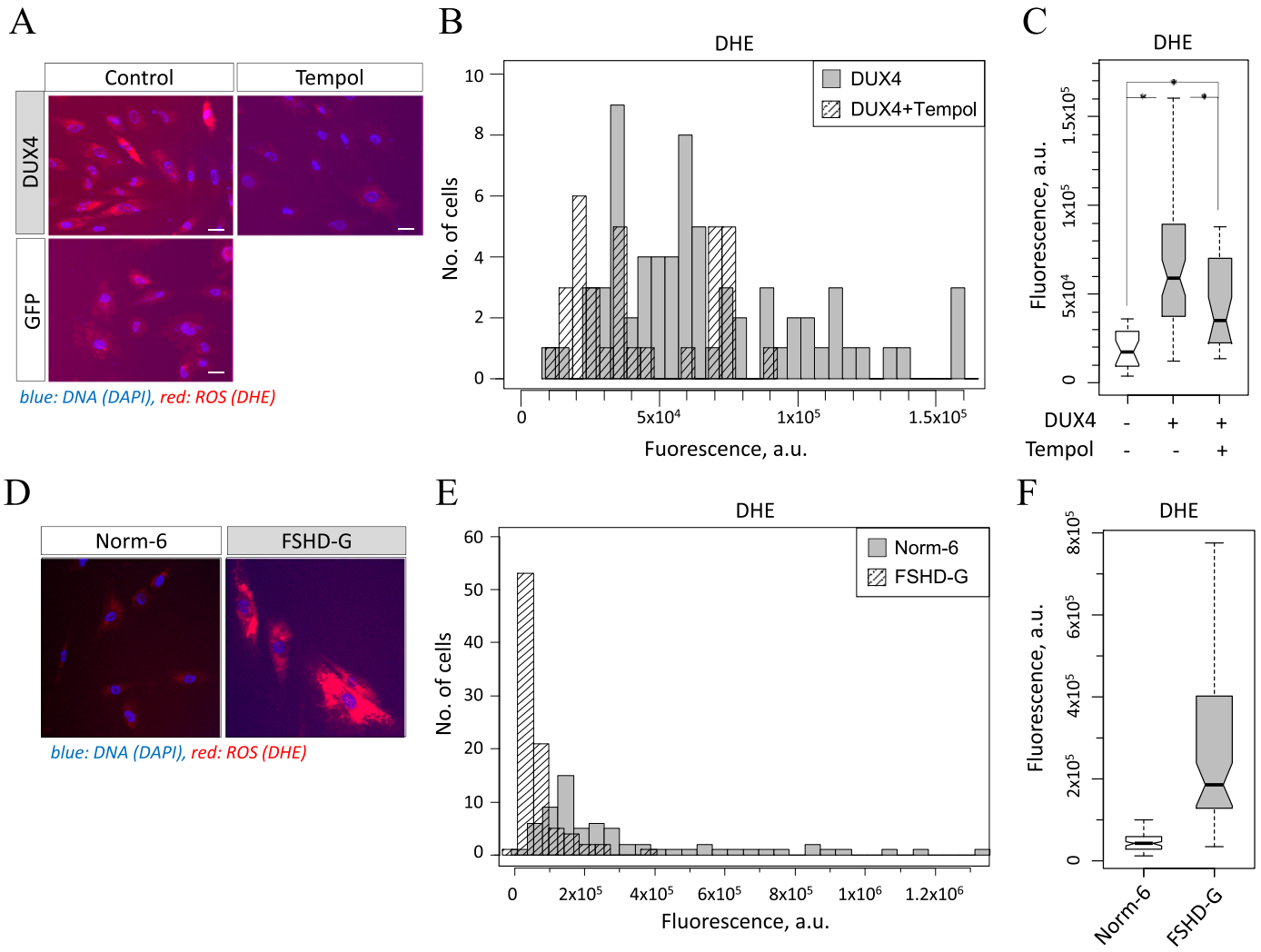

Fig. 6. Oxidative stress in FSHD primary myoblasts and in *DUX4*-transfected human myoblasts. **A**. Immunofluorescent imaging of human immortalized myoblasts transfected with pCI-Neo-DUX4 or control plasmid (phrGFP-N1), treated or not with tempol and stained with a fluorescent ROS sensor probe dihydroethidium (DHE); representative images are shown, 20X magnification, bar = 10 μm. **B**. Effect of tempol on the distribution of DHE fluorescence intensity in human immortalized myoblasts transfected with *DUX4*, 33 cells analyzed for "+tempol" condition and 69 cells - for "-tempol" condition. **C**. Statistical analysis of DHE fluorescence intensity distribution of samples shown on **A**. (*) *t*-test p-value < 0.05. Notches indicate a confidence interval. **D**. Reactive oxygen species (ROS) visualization via DHE fluorescence analysis in primary myoblasts from the FSHD patient FSHD-G and a healthy subject Norm-6; representative images are shown, 20X magnification, bar = 10 μm. **E**. Distribution of DHE intensity in myoblasts from the FSHD patient FSHD-G (68 cells analyzed) and a healthy subject Norm-6 (89 cells analyzed) and its statistical analysis (**F**) (*) *t*-test p-value < 0.05.

and preserved in liquid nitrogen for future use. After unfreezing, the myoblasts were cultured for one more passage in high-glucose DMEM (here and below Sigma #D6546) supplemented with 10% FBS (Millerium #BWSTS1810/500), 1% Ultroser G (Biosepra #15950–017), 4 mM L-glutamine (Sigma #68540–25G), 50 μg/mL gentamicin (Sigma #G1397) and 1 μg/mL Amphotericin B (Fungizone, Gibco #15290–018) and then switched to the proliferation medium (DMEM, 20% FBS, 4 mM L-glutamine, 50 μg/mL gentamicin1 μg/mL Amphotericin), passaged at a cell confluency not exceeding 30% and used for transfection and tests up to passage 10 to avoid cellular senescence and spontaneous differentiation. To induce the myogenic differentiation, the myoblasts were grown to confluency in proliferating medium, switched to differentiation medium (DMEM, 2% FBS, 4 mM L-glutamine, 50 μg/mL gentamicin 1 μg/mL Amphotericin) and cultured for 6 days without medium change. pMyo were cultured in cell culture dishes coated with collagen using sterile a 0.1% solution of collagen powder (Sigma #C7661) in 0.2% acetic acid.

Human immortalized myoblasts LHCN-M2 derived from a healthy subject ("iMyo") (a kind gift from Dr. V. Mouly, Institute of Myology, Paris) were cultured in the media composed of 4 parts of high-glucose DMEM, 1 part of Medium 199 (Sigma #M4530) and supplemented with 20% FBS, 1X penicillin/streptomycin (Gibco #15140–122) and 2.5 μg/mL plasmocin (Invivogen #MPP-35–02).

The rhabdomyosarcoma cell line TE-671 (a kind gift from Dr. S. Leibowitz, Institut Gustave Roussy, France) was cultured in DMEM supplemented with 10% FBS, 2 mM L-glutamine, 100 units/mL Penicillin G, 100 μg/mL Streptomycin sulfate (Gibco #15070–063) and 1 μg/mL Amphotericin B.

pMyo were transfected using 4 μL of siPORTNeoFX and 10 nM DUX4 siRNA mix or control siRNA using a "reverse" transfection schema as previously described [38]. iMyo transfection was carried out in 6-well plates. 200,000 cells in 1 mL of culturing medium were mixed with 200 μL of OptiMEM (Gibco #31985062) containing 600 ng of plasmid DNA and 0.6 μL Lipofectamine 2000 (Invitrogen #11668–019) per well using a "reverse" transfection schema.

24 h prior to transfection, TE-671 cells were plated in a 6 well plate at the density 2.5×10^5 cells/well and then transfected using 3 μg of plasmid DNA and 6 μL JetPEI (Polyplus #101–10) in 300 μL of 150 mM NaCl per well.

To overexpress DUX4, the plasmid pCI-NeoDUX4 containing the ORF of human *DUX4* gene under control of the CMV promoter

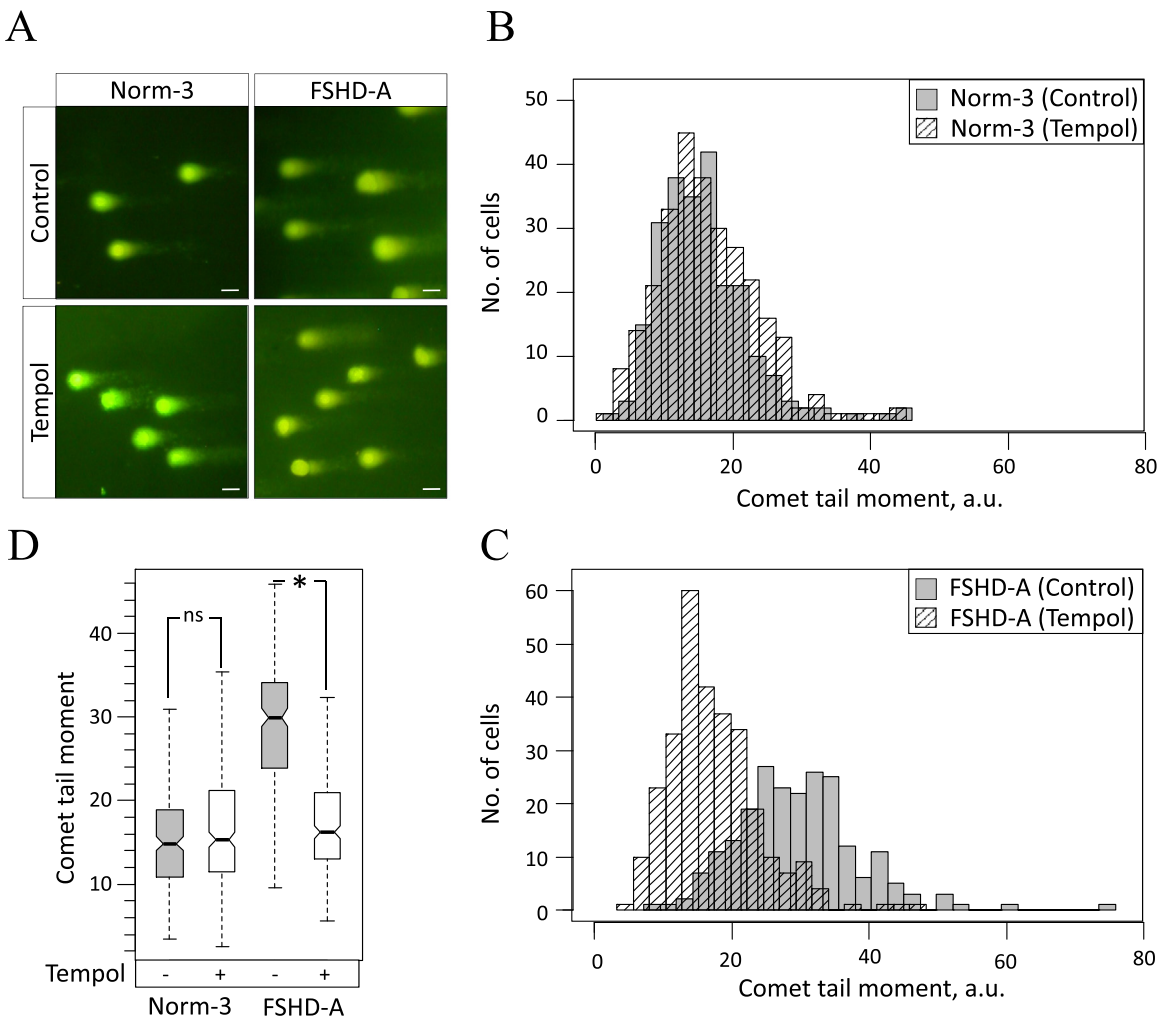

Fig. 7. Effect of the antioxidant addition to the culture medium on the constitutive DNA damage in FSHD myoblasts. **A**. DNA integrity of primary myoblasts from the FSHD patient FSHD-A and a normal subject Norm-3 cultured in the medium supplemented or not with 100 μM of tempol was analyzed using comet assay in alkaline conditions, representative images with 20X magnification are shown. **B,C**. Effect of the culture medium supplementation with 100 μM tempol on the distribution of comet tail moments in normal myoblasts (Norm-3, 207 untreated and 284 tempol-treated cells analyzed) (**B**) and FSHD myoblasts (FSHD-A, 224 untreated and 293 tempol-treated cells analyzed) (**C**). **D**. Statistical analysis of distributions shown in panels B and C; (*) *t*-test p-value < 0.05.; ns – non-significant.

(a kind gift from Alexandra Belayew and Frederique Coppée, University of Mons, Belgium) was used; as a control pCI-Neo (Promega) and phrGFP-N1 (Stratagen) plasmids were used.

To test the effect of tempol on the level of DNA damage in pMyo, the culture medium was supplemented with 100 μM tempol (Enzo Life Sciences #ALX-430–081) or DMSO as a control (in water) 2 days before the DNA damage analysis; the medium was replaced every 24 h. To test the effect of tempol on the level of DNA damage in iMyo, the culture medium was supplemented with 100 μM tempol 3 h before the transfection; the tempol treatment was renewed 24 h after the transfection, and the DNA damage analysis was carried out 48 h post-transfection.

4.2. Immunofluorescence staining and quantification

Proliferating pMyo were, fixed with 2% PFA (Euromedex) for 5 min, permeabilized with 0.25% Triton X-100 (Sigma-Aldrich) for 5 min, blocked with 0.5% BSA (Euromedex), incubated with mouse monoclonal antibodies against γH2AX (phospho Ser139 H2AX Active Motif #39117, 1:500) or mouse monoclonal anti-Troponin T (Sigma # T6277, 1:50) for 1 h, stained with Alexa Fluor 488 anti-mouse IgG (Life Technologies #A-21200, 1:100) for 1 h, mounted with a mounting medium containing DAPI (Vector laboratories) and observed under a fluorescent microscope (Microvision instruments, excitation/emission: 488/519 nm, green fluorescence). To create a full image of the specimen, images of adjacent fields were stitched together using Cartograph software (Microvision). For γH2AX and DUX4 co-staining, proliferating iMyo transfected with pCI-NeoDUX4 or phrGFP-N1 were incubated simultaneously with a mouse monoclonal antibody against DUX4 (9A12 kindly donated by Alexandra Belayew, University of Mons, Belgium) and rabbit polyclonal antibodies against γH2AX (phospho Ser139 H2AX Active Motif #39117, 1:500), stained with Alexa Fluor 488-conjugated anti-mouse IgG (Life Technologies#A-21200, 1:100, excitation/emission: 488/519 nm, green fluorescence) and Alexa Fluor 514-conjugated anti-rabbit IgG (Life Technologies #A-31558, 1:100, excitation/emission: 518/540 nm, red fluorescence).

4.3. ROS staining in living cells

48 h after the transfection, iMyo were incubated in a 5 mM DHE-containing ROS staining solution diluted 1:8000 in the 1X proprietary assay buffer (Muse oxidative stress kit, Millipore) for 15 min in the dark at room temperature with shaking, washed three times with PBS, mounted using a DAPI mounting medium (Vector laboratories), observed under a fluorescent microscope (excitation/emission: 520/610 nm, red fluorescence). Images from adjacent fields of view were stitched together by using the

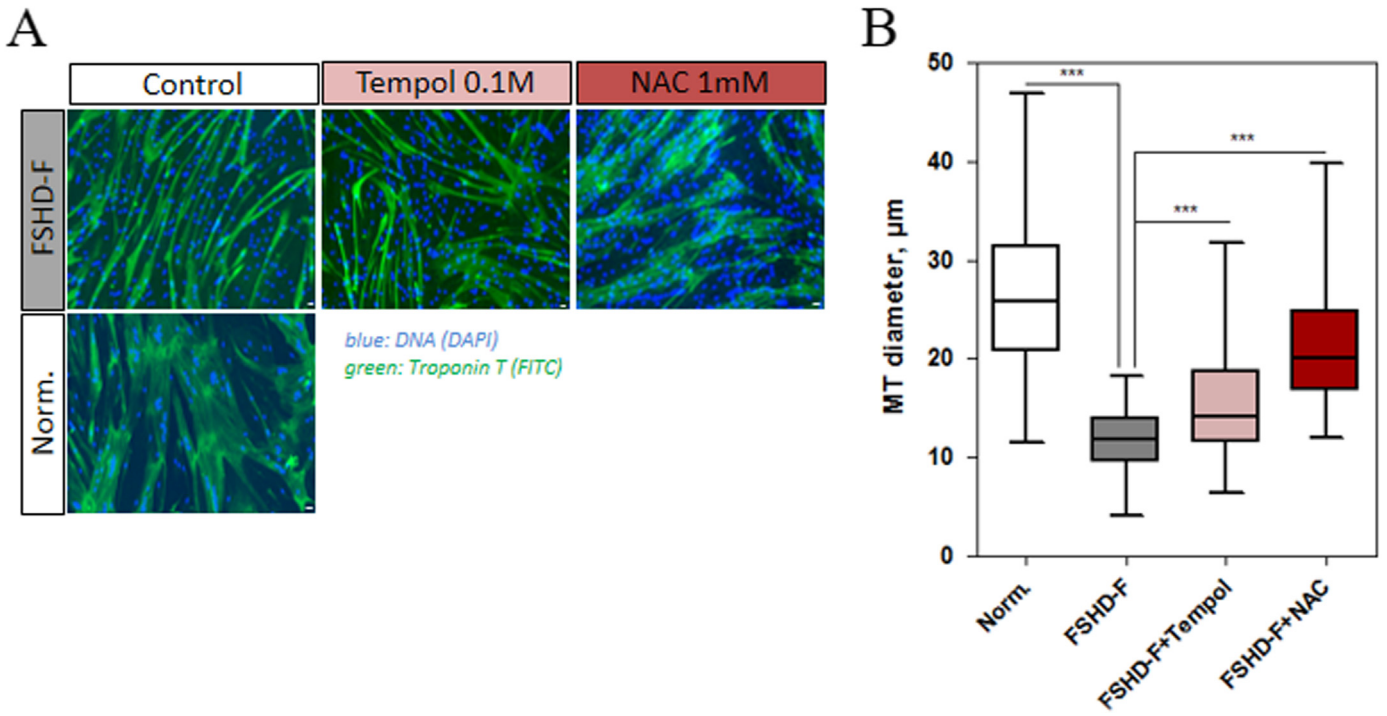

Fig. 8. Effect of the antioxidants on the morphology of FSHD myotubes. **A**. Immunofluorescent imaging of myotubes (MT) derived from atrophic (FSHD-F) primary myoblasts isolated from an FSHD patient or a healthy control (Norm-7); green: Troponin T, blue: DAPI. 10X magnification, bar = 10 μm. Full-size images are shown on Supplementary Fig. S8. **B.** Statistical analysis of diameter measurements of normal and FSHD-F myotubes before and after antioxidant treatment; (***) *t*-test p-value < 0.001.

Cartograph software (Microvision) to create one large image of the specimen. The fluorescence of at least 100 cells per sample was quantified with ImageJ (NIH) using the formula: CTCF (corrected total cell fluorescence)= Integrated_Density - (Area_of_selected _cell X Mean_fluorescence_of_background_readings).

4.4. Measurement of H_2O_2 generation

H_2O_2 generation was quantified by the Amplex red/horseradish peroxidase assay (Sigma Aldrich), which detects the accumulation of a fluorescent oxidized product, according to a previously published protocol [42]. Cells (5.10^4) in Dulbecco's phosphate-buffered saline (D-PBS) with CaCl2 and MgCl2 were incubated with D-glucose (1 mg/mL), horseradish peroxidase (0.5 U/mL; Roche), and Amplex red (50 μM; Sigma Aldrich), and immediately the fluorescence was measured in a microplate reader (Victor3; PerkinElmer) at 37 °C for 1 h using excitation at 530 nm and emission at 595 nm. H_2O_2 release was quantified (nanomoles H_2O_2 per hour per 10^5 cells) using standard calibration curves.

4.5. Western blot

Whole cell protein extracts were prepared from frozen myoblast cell pellets using TENT buffer (150 mM NaCl, 1 mM EDTA, 50 mM Tris-HCl pH7.5, 0.5% NP-40) [58] supplemented with anti-protease and anti-phosphatase inhibitor cocktails (Roche #04693159001, #04906845001), separated on 15% (for γH2AX and H2B staining) or 8% polyacrylamide gel depending on the protein molecular weight, transferred to a nitrocellulose membrane, blocked with 5% BSA/PyTBST (for staining of phosphorylated proteins) or 5% milk/PyTBST, hybridized with primary antibodies against γH2AX (phospho Ser139 H2AX #ab11174, Abcam), H2B (SantaCruz #sc8650), Actin (Millipore #mab1501), washed with 1X PyTBST (10 mM Tris-HCl pH7.4, 75 mM NaCl, 1 mM EDTA, 0.1% Tween 20) [59] to reduce background, hybridized with secondary antibodies conjugated to HRP (SantaCruz #sc2030, #sc2768, #sc2005), revealed with ECL+(GE Healthcare), exposed to X-ray film (Amersham) and developed in the chemical film processor (FujiFilm). Quantification of scanned X-ray images was performed using ImageJ.

4.6. FACS analysis

Proliferating pMyo were cultured for 5 h, as described above in the presence of 10 μM BrdU (Sigma #B5002–100G) freshly dissolved in PBS, trypsinized, centrifuged, resuspended in PBS and fixed at 4 °C overnight in 60% Ethanol at a final concentration of 1×10^6 cells/mL, the DNA was then denatured in 2 N HCl for 20 min at 37 °C, neutralized with 500 mM of sodium borate, washed with PBTB (PBS supplemented with 0.5% Tween20 and 0.5% BSA), incubated with *anti*-BrdU antibodies (Sigma #B8434, 2 μg/μL, 1:100) in 100 μL of PBTB for 1 h at room temperature in the dark, diluted 10-fold with PBTB, centrifuged, incubated for 1 h at room temperature in the dark with anti-mouse antibody conjugated to Alexa Fluor 488 (Invitrogen #A11059, 2 mg/mL, 1:200) diluted 10-fold with PBTB, centrifuged, resuspended in 500 μL of PBTB, stained with 10 μg/mL of PI for 15 min at room temperature in the dark and treated with 20 μg/mL of RNAse I for 30 min. Cell cycle distribution data were obtained using FACS Calibur (BD Bioscience) and analyzed using FCS Express v3.

4.7. Apurinic/apyrimidinic site quantification

Genomic DNA was isolated using Nucleospin Tissue kit (Macherey Nagel). AP sites were quantified using DNA damage colorimetric assay kit (Abcam #ab65353) as instructed by the producer. Briefly, 500 ng of genomic DNA were labeled with aldehyde-reactive probe (ARP) containing a biotin moiety, immobilized in microwells, incubated with streptavidin-conjugated HRP; following an HRP substrate addition, the absorbance (650 nm) was

measured using a microplate absorbance reader. To translate the absorbance units into the number of AP sites, a standard curve was obtained using control DNA containing 40 AP sites per 10^5 bp.

4.8. Alkaline Comet assay and scoring for DNA damage

The alkaline comet assay was performed using the Trevigen CometAssay kit (Trevigen # 4,250,050-k) and 20-well CometSlide™ (Trevigen # 4252–500-01). Briefly, the cells were combined at 1×10^5/mL with a molten low melting point agarose (LMAgarose) at 37 °C at the ratio of 1/10 (v/v) and 50 μL were deposed onto a 20-well pre-coated CometSlide™. The agarose was allowed to solidify by placing the slides flat at 4 °C in the dark for 15 min. The slides were then immersed in a pre-chilled lysis solution (Trevigen # 4250–050-01) for 1 h at 4 °C to remove the membrane, cellular proteins and histones. Following lysis, DNA unwinding was completed by incubating the slides in a freshly prepared alkaline unwinding solution (200 mM NaOH, 1 mM EDTA pH > 13) for 1 h at room temperature. The slides were then subjected to electrophoresis at 21 V for 30 min at 4 °C in the same alkaline solution, washed twice with dH_2O for 5 min each, washed in 70% ethanol for 5 min, dried at 37 °C for 30 min, and stained with 50 μL of diluted SYBR Green solution (1/10,000 in TE buffer pH 7.5, Trevigen # 4250–050-05). The slides were allowed to dry completely at room temperature before observation under the epifluorescence microscope (Microvision instruments, Excitation/Emission: 494/521 nm, 20X zoom). Images of 100 randomly selected non-overlapping cells were captured and analyzed using Tritek CometScore software. A variety of measurements including the percentage of DNA in the tail (expressed as % of total DNA), the tail length (measured from the leading edge of the comet head) and tail moment (the measure of tail length multiplied by tail intensity) were calculated to evaluate the extent of DNA damage. Mean values from at least 100 nuclei were used in calculations. All steps were conducted in the dark to minimize extraneous sources of DNA damage.

4.9. Myogenic differentiation and myotubes quantification

Myoblasts from normal and FSHD primary cell lines were seeded at a density of 3.10^5 cells per 10 cm collagen-coated petri dishes, and cultured in 10 mL of proliferation medium supplemented with 100 μM of tempol, 1 mM N-Acetyl-L-cysteine (NAC) (Sigma #A7250) or DMSO (control). 48 h later the cells were collected, washed and seeded in 35 mm collagen-coated petri dishes (80–100% confluence) under proliferation conditions. Myogenic differentiation was then induced 4 h later by replacing the growth medium with differentiation medium, supplemented or not with 100 μM tempol or 1 mM NAC. The differentiation medium was replaced every 72 h to ensure a constant antioxidant concentration. The cells were kept 6 days under differentiation conditions and were then fixed and immuno-stained with anti-Troponin T primary antibody, as described previously. The diameter of atrophic myotubes was measured using ImageJ software. For each myotube the mean value of three diameter measurements at three different points was calculated in μm. At least 100 myotubes were counted per condition.

4.10. Transcriptome profiling

RNA was prepared using organic extraction and ethanol precipitation as described [60] followed by silica column cleanup using Nucleospin RNA Extraction kit (Macherey Nagel). RNA extracted from pMyo isolated from 6 FSHD patients and 5 healthy individuals (biological replicates) was Cy3-labeled, mixed with a pool of RNA samples labeled with Cy5 and hybridized to Gene Expression microarrays (4×44k #G4112F, Agilent) and scanned as instructed by the manufacturer. Scanned images were then analyzed using the Feature Extraction software (Agilent) and the gene expression data were treated in R and Bioconductor. Spots with intensity lower than 50 or lower than background in more than 50% of biological replicates have been removed from further analysis. The background correction and intensity normalization procedures were applied for the remaining ~30 000 probes using the Bioconductor package vsn [61]. A background offset and a scaling factor for each array and dye channel were calculated using the least squares regression procedure, then a generalized log-transformation was applied. To determine the differentially expressed genes, a *t*-test analysis was applied using the limma package from Bioconductor [61]. Using this package, a linear model is fitted to the expression data for each gene. An empirical Bayes moderation of the standard errors was performed. This analysis resulted in the identification of 512 and 94 significant Agilent ID in FSHD myoblasts and myotubes respectively. Gene symbols and descriptions corresponding to significant Agilent IDs were retrieved from the Agilent microarray annotation file and db2db and DAVID gene ID conversion tools. In case of disagreement between the sources, HGNC database (http://www.genenames.org/) was consulted. In total, 504 and 141 unique genes were differentially expressed in FSHD myoblasts and myotubes respectively; 400 and 109 genes were protein-coding.

4.11. Functional annotation of differentially expressed genes

Protein-coding genes differentially expressed in FSHD myoblasts and myotubes were used for functional annotation with DAVID (http://david.abcc.ncifcrf.gov/) using GOTERM_BP_FAT list and the default background. The stringency of functional annotation clustering was set to "medium". To establish a reliable threshold of significant functional clusters, we generated random lists of 266, 75, 52 and 27 genes corresponding to the number of genes up- and downregulated in FSHD myoblasts and myotubes, functionally annotated them with DAVID and used the most significant p-values and FDRs as thresholds. Significant functional clusters were then manually assembled into superclusters using Microsoft Excel with Ablebits add-ons (https://www.ablebits.com/).

4.12. Statistical analysis

Tail moment data for Comet assay have been compared using single-factor ANOVA incorporating 75th percentile as a characteristic of a tail moment distribution according to recommendation in [62]. Mann-Whitney test was performed using R function wilcox.test. Student's *t*-test was performed using Excel function *T* TEST, a p-value of 0.05 was considered statistically significant. Statistical power was calculated using http://powerandsamplesize.com/. Kruskal-Wallis test on Tail moment distributions was performed using kruskal.test function in R. The number of experiments and samples on which statistical analysis were performed are indicated in each experiment.

4.13. RT-PCR

RNA was prepared using organic extraction and ethanol precipitation as described [60]. Reverse transcription and PCR amplification of DUX4 were carried out as described in detail previously [38].

4.14. Microarray validation

Total RNA was isolated from 2×10^6 myoblasts, or myotubes using

Trizol (Invitrogen) and reverse transcribed using the High Capacity cDNA Archive kit (Applied Biosystems) according to the manufacturer protocol, mixed with 2x Taqman PCR mix (Applied Biosystems) and analyzed via qPCR on Abiprism 7900HT using Taqman Low Density Array (TLDA) (Applied Biosystems) charged with the following probes: BLM, Hs00172060_m1; CCNB1, Hs01030101_g1; CDC25C, Hs00156407_m1; E2F1, Hs00153451_m1; KIF20A, Hs00993573_m1; MPP4, Hs00608861_m1; PLK1, Hs00983227_m1; RNASEH2A, Hs00197370_m1; RRM2, Hs00357247_g1; TRAIP, Hs00183394_m1; CCNA, Hs00996789_g1; TRIM43, Hs00299174_m1; PRAMEF2, Hs00363780_m1; MBD3L2, Hs00544743_m1. Expression was analyzed using ΔΔCt method using GAPDH, Hs03929097_g1.

5. Conflict of interest

The authors declare no conflict of interest.

Acknowledgments

This research was supported by the MEGAFSHD grant from the Association Française contre les Myopathies (AFM) to YSV and the Grant no. 16–54-16015 from the Russian Foundation for Basic Research to VZ. We thank Dr. Dalila Laoudj-Chenivesse for primary myoblasts and Ms. Shirmoné Botha for critical reading of the manuscript.

Appendix A. Supplementary material

Supplementary data associated with this article can be found in the online version at http://dx.doi.org/10.1016/j.freeradbiomed.2016.08.007.

References

[1] J.C. Deenen, H. Arnts, S.M. van der Maarel, G.W. Padberg, J.J. Verschuuren, E. Bakker, S.S. Weinreich, A.L. Verbeek, B.G. van Engelen, Population-based incidence and prevalence of facioscapulohumeral dystrophy, Neurology 83 (12) (2014) 1056–1059.
[2] M. Richards, F. Coppee, N. Thomas, A. Belayew, M. Upadhyaya, Facioscapulohumeral muscular dystrophy (FSHD): an enigma unravelled? Hum. Genet 131 (3) (2012) 325–340.
[3] D.S. Cabianca, D. Gabellini, The cell biology of disease: FSHD: copy number variations on the theme of muscular dystrophy, J. Cell Biol. 191 (6) (2010) 1049–1060.
[4] M. Bakay, Z. Wang, G. Melcon, L. Schiltz, J. Xuan, P. Zhao, V. Sartorelli, J. Seo, E. Pegoraro, C. Angelini, B. Shneiderman, D. Escolar, Y.W. Chen, S.T. Winokur, L. M. Pachman, C. Fan, R. Mandler, Y. Nevo, E. Gordon, Y. Zhu, Y. Dong, Y. Wang, E. P. Hoffman, Nuclear envelope dystrophies show a transcriptional fingerprint suggesting disruption of Rb-MyoD pathways in muscle regeneration, Brain 129 (Pt 4) (2006) 996–1013.
[5] B. Celegato, D. Capitanio, M. Pescatori, C. Romualdi, B. Pacchioni, S. Cagnin, A. Vigano, L. Colantoni, S. Begum, E. Ricci, R. Wait, G. Lanfranchi, C. Gelfi, Parallel protein and transcript profiles of FSHD patient muscles correlate to the D4Z4 arrangement and reveal a common impairment of slow to fast fibre differentiation and a general deregulation of MyoD-dependent genes, Proteomics 6 (19) (2006) 5303–5321.
[6] P.G. van Overveld, R.J. Lemmers, L.A. Sandkuijl, L. Enthoven, S.T. Winokur, F. Bakels, G.W. Padberg, G.J. van Ommen, R.R. Frants, S.M. van der Maarel, Hypomethylation of D4Z4 in 4q-linked and non-4q-linked facioscapulohumeral muscular dystrophy, Nat. Genet. 35 (4) (2003) 315–317.
[7] S.T. Winokur, Y.W. Chen, P.S. Masny, J.H. Martin, J.T. Ehmsen, S.J. Tapscott, S. M. van der Maarel, Y. Hayashi, K.M. Flanigan, Expression profiling of FSHD muscle supports a defect in specific stages of myogenic differentiation, Hum. Mol. Genet. 12 (22) (2003) 2895–2907.
[8] D. Laoudj-Chenivesse, G. Carnac, C. Bisbal, G. Hugon, S. Bouillot, C. Desnuelle, Y. Vassetzky, A. Fernandez, Increased levels of adenine nucleotide translocator 1 protein and response to oxidative stress are early events in facioscapulohumeral muscular dystrophy muscle, J. Mol. Med. 83 (3) (2005) 216–224.
[9] R.J. Osborne, S. Welle, S.L. Venance, C.A. Thornton, R. Tawil, Expression profile of FSHD supports a link between retinal vasculopathy and muscular dystrophy, Neurology 68 (8) (2007) 569–577.
[10] P. Arashiro, I. Eisenberg, A.T. Kho, A.M. Cerqueira, M. Canovas, H.C. Silva, R. C. Pavanello, S. Verjovski-Almeida, L.M. Kunkel, M. Zatz, Transcriptional regulation differs in affected facioscapulohumeral muscular dystrophy patients compared to asymptomatic related carriers, Proc. Natl. Acad. Sci. USA 106 (15) (2009) 6220–6225.
[11] S. Cheli, S. Francois, B. Bodega, F. Ferrari, E. Tenedini, E. Roncaglia, S. Ferrari, E. Ginelli, R. Meneveri, Expression profiling of FSHD-1 and FSHD-2 cells during myogenic differentiation evidences common and distinctive gene dysregulation patterns, PloS One 6 (6) (2011) e20966.
[12] K. Tsumagari, S.C. Chang, M. Lacey, C. Baribault, S.V. Chittur, J. Sowden, R. Tawil, G.E. Crawford, M. Ehrlich, Gene expression during normal and FSHD myogenesis, BMC Med. Genom. 4 (2011) 67.
[13] F. Rahimov, O.D. King, D.G. Leung, G.M. Bibat, C.P. Emerson Jr., L.M. Kunkel, K. R. Wagner, Transcriptional profiling in facioscapulohumeral muscular dystrophy to identify candidate biomarkers, Proc. Natl. Acad. Sci. USA 109 (40) (2012) 16234–16239.
[14] G. Tasca, M. Pescatori, M. Monforte, M. Mirabella, E. Iannaccone, R. Frusciante, T. Cubeddu, F. Laschena, P. Ottaviani, E. Ricci, Different molecular signatures in magnetic resonance imaging-staged facioscapulohumeral muscular dystrophy muscles, PloS One 7 (6) (2012) e38779.
[15] A. Tassin, B. Leroy, D. Laoudj-Chenivesse, A. Wauters, C. Vanderplanck, M.C. Le Bihan, F. Coppee, R. Wattiez, A. Belayew, FSHD myotubes with different phenotypes exhibit distinct proteomes, PloS One 7 (12) (2012) e51865.
[16] P. Dmitriev, U. Kairov, T. Robert, A. Barat, V. Lazar, G. Carnac, D. Laoudj-Chenivesse, Y.S. Vassetzky, Cancer-related genes in the transcription signature of facioscapulohumeral dystrophy myoblasts and myotubes, J. Cell Mol. MEd 18 (2) (2014) 208–217.
[17] P. Dmitriev, L. Stankevicins, E. Ansseau, A. Petrov, A. Barat, P. Dessen, T. Robert, A. Turki, V. Lazar, E. Labourer, A. Belayew, G. Carnac, D. Laoudj-Chenivesse, M. Lipinski, Y.S. Vassetzky, Defective regulation of microRNA target genes in myoblasts from facioscapulohumeral dystrophy patients, J. Biol. Chem. 288 (49) (2013) 34989–35002.
[18] C. Dib, Y.B. Saada, P. Dmitriev, C. Richon, P. Dessen, D. Laoudj-Chenivesse, G. Carnac, M. Lipinski, Y.S. Vassetzky, Correction of the FSHD Myoblast Differentiation Defect by Fusion With Healthy Myoblasts, J Cell Physiol (2015).
[19] M. Barro, G. Carnac, S. Flavier, J. Mercier, Y. Vassetzky, D. Laoudj-Chenivesse, Myoblasts from affected and non-affected FSHD muscles exhibit morphological differentiation defects, J. Cell Mol. Med. 14 (1–2) (2010) 275–289.
[20] S.T. Winokur, K. Barrett, J.H. Martin, J.R. Forrester, M. Simon, R. Tawil, S. A. Chung, P.S. Masny, D.A. Figlewicz, Facioscapulohumeral muscular dystrophy (FSHD) myoblasts demonstrate increased susceptibility to oxidative stress, Neuromuscul. Disord. 13 (4) (2003) 322–333.
[21] V. Sharma, N. Harafuji, A. Belayew, Y.W. Chen, DUX4 differentially regulates transcriptomes of human rhabdomyosarcoma and mouse C2C12 cells, PloS One 8 (5) (2013) e64691.
[22] A. Turki, M. Hayot, G. Carnac, F. Pillard, E. Passerieux, S. Bommart, E. Raynaud de Mauverger, G. Hugon, J. Pincemail, S. Pietri, K. Lambert, A. Belayew, Y. Vassetzky, R. Juntas Morales, J. Mercier, D. Laoudj-Chenivesse, Functional muscle impairment in facioscapulohumeral muscular dystrophy is correlated with oxidative stress and mitochondrial dysfunction, Free Radic. Biol. Med 53 (553) (2012) 1068–1079.
[23] A. Musaro, S. Fulle, G. Fano, Oxidative stress and muscle homeostasis, Curr. Opin. Clin. Nutr. Metab. Care 13 (3) (2010) 236–242.
[24] E. Barbieri, P. Sestili, Reactive oxygen species in skeletal muscle signaling, J. Signal. Transduct. 2012 (2012) 982794.
[25] E. Marzetti, J.C. Hwang, H.A. Lees, S.E. Wohlgemuth, E.E. Dupont-Versteegden, C.S. Carter, R. Bernabei, C. Leeuwenburgh, Mitochondrial death effectors: relevance to sarcopenia and disuse muscle atrophy, Biochim. Biophys. Acta 1800 (3) (2010) 235–244.
[26] M. Bar-Shai, E. Carmeli, A.Z. Reznick, The role of NF-kappa B in protein breakdown in immobilization, aging, and exercise: from basic processes to promotion of health, Ann. NY Acad. Sci. 1057 (2005) 431–447.
[27] D. Bosnakovski, Z. Xu, E.J. Gang, C.L. Galindo, M. Liu, T. Simsek, H.R. Garner, S. Agha-Mohammadi, A. Tassin, F. Coppee, A. Belayew, R.R. Perlingeiro, M. Kyba, An isogenetic myoblast expression screen identifies DUX4-mediated FSHD-associated molecular pathologies, EMBO J. 27 (20) (2008) 2766–2779.
[28] S.P. Jackson, J. Bartek, The DNA-damage response in human biology and disease, Nature 461 (7267) (2009) 1071–1078.
[29] M. O'Driscoll, Diseases associated with defective responses to DNA damage, Cold Spring Harb. Perspect. Biol. 4 (12) (2012).
[30] W.M. Schmidt, M.H. Uddin, S. Dysek, K. Moser-Thier, C. Pirker, H. Hoger, I. M. Ambros, P.F. Ambros, W. Berger, R.E. Bittner, DNA damage, somatic aneuploidy, and malignant sarcoma susceptibility in muscular dystrophies, PLoS Genet. 7 (4) (2011) e1002042.
[31] A. Fanzani, E. Monti, R. Donato, G. Sorci, Muscular dystrophies share pathogenetic mechanisms with muscle sarcomas, Trends Mol. MEd 19 (9) (2013) 546–554.
[32] N.P. Singh, M.T. McCoy, R.R. Tice, E.L. Schneider, A simple technique for quantitation of low levels of DNA damage in individual cells, Exp. Cell Res. 175 (1) (1988) 184–191.
[33] R.R. Tice, P.W. Andrews, N.P. Singh, The single cell gel assay: a sensitive technique for evaluating intercellular differences in DNA damage and repair, Basic Life Sci. 53 (1990) 291–301.
[34] R.R. Tice, E. Agurell, D. Anderson, B. Burlinson, A. Hartmann, H. Kobayashi, Y. Miyamae, E. Rojas, J.C. Ryu, Y.F. Sasaki, Single cell gel/comet assay:

guidelines for in vitro and in vivo genetic toxicology testing, Environ. Mol. Mutagen 35 (3) (2000) 206–221.
[35] J.T. Vilquin, J.P. Marolleau, S. Sacconi, I. Garcin, M.N. Lacassagne, I. Robert, B. Ternaux, B. Bouazza, J. Larghero, C. Desnuelle, Normal growth and regenerating ability of myoblasts from unaffected muscles of facioscapulohumeral muscular dystrophy patients, Gene Ther. 12 (22) (2005) 1651–1662.
[36] R. Morosetti, M. Mirabella, C. Gliubizzi, A. Broccolini, C. Sancricca, M. Pescatori, T. Gidaro, G. Tasca, R. Frusciante, P.A. Tonali, G. Cossu, E. Ricci, Isolation and characterization of mesoangioblasts from facioscapulohumeral muscular dystrophy muscle biopsies, Stem Cells 25 (12) (2007) 3173–3182.
[37] R. Morosetti, T. Gidaro, A. Broccolini, C. Gliubizzi, C. Sancricca, P.A. Tonali, E. Ricci, M. Mirabella, Mesoangioblasts from facioscapulohumeral muscular dystrophy display in vivo a variable myogenic ability predictable by their in vitro behavior, Cell Transplant. 20 (8) (2011) 1299–1313.
[38] C. Vanderplanck, E. Ansseau, S. Charron, N. Stricwant, A. Tassin, D. Laoudj-Chenivesse, S.D. Wilton, F. Coppee, A. Belayew, The FSHD atrophic myotube phenotype is caused by DUX4 expression, PloS One 6 (10) (2011) e26820.
[39] V. Kowaljow, A. Marcowycz, E. Ansseau, C.B. Conde, S. Sauvage, C. Matteotti, C. Arias, E.D. Corona, N.G. Nunez, O. Leo, R. Wattiez, D. Figlewicz, D. Laoudj-Chenivesse, A. Belayew, F. Coppee, A.L. Rosa, The DUX4 gene at the FSHD1A locus encodes a pro-apoptotic protein, Neuromuscul. Disord. 17 (8) (2007) 611–623.
[40] L.M. Wallace, S.E. Garwick, W. Mei, A. Belayew, F. Coppee, K.J. Ladner, D. Guttridge, J. Yang, S.Q. Harper, DUX4, a candidate gene for facioscapulohumeral muscular dystrophy, causes p53-dependent myopathy in vivo, Ann. Neurol. 69 (3) (2011) 540–552.
[41] R.D. Wuebbles, S.W. Long, M.L. Hanel, P.L. Jones, Testing the effects of FSHD candidate gene expression in vertebrate muscle development, Int J. Clin. Exp. Pathol. 3 (4) (2010) 386–400.
[42] A. Carre, R.A. Louzada, R.S. Fortunato, R. Ameziane-El-Hassani, S. Morand, V. Ogryzko, D.P. de Carvalho, H. Grasberger, T.L. Leto, C. Dupuy, When an Intramolecular Disulfide Bridge Governs the Interaction of DUOX2 with Its Partner DUOXA2, Antioxid. Redox Signal. 23 (9) (2015) 724–733.
[43] Y. Morel, R. Barouki, Repression of gene expression by oxidative stress, Biochem J. 342 (Pt 3) (1999) 481–496.
[44] M. Zafarullah, W.Q. Li, J. Sylvester, M. Ahmad, Molecular mechanisms of N-acetylcysteine actions, Cell Mol. Life Sci. 60 (1) (2003) 6–20.
[45] K. Arahata, T. Ishihara, H. Fukunaga, S. Orimo, J.H. Lee, K. Goto, I. Nonaka, Inflammatory response in facioscapulohumeral muscular dystrophy (FSHD): immunocytochemical and genetic analyses, Muscle Nerve Suppl. (2) (1995) S56–S66.
[46] A. Pakula, J. Schneider, J. Janke, U. Zacharias, H. Schulz, N. Hubner, A. Mahler, A. Spuler, S. Spuler, P. Carlier, M. Boschmann, Altered expression of cyclin A 1 in muscle of patients with facioscapulohumeral muscle dystrophy (FSHD-1), PloS One 8 (9) (2013) e73573.
[47] D.M. DeMarini, Genotoxicity of tobacco smoke and tobacco smoke condensate: a review, Mutat. Res 567 (2–3) (2004) 447–474.
[48] R.P. Rastogi, Richa, A. Kumar, M.B. Tyagi, R.P. Sinha, Molecular mechanisms of ultraviolet radiation-induced DNA damage and repair, J. Nucleic Acids 2010 (2010) 592980.
[49] R. De Bont, N. van Larebeke, Endogenous DNA damage in humans: a review of quantitative data, Mutagenesis 19 (3) (2004) 169–185.
[50] A. Mazouzi, G. Velimezi, J.I. Loizou, DNA replication stress: causes, resolution and disease, Exp. Cell Res 329 (1) (2014) 85–93.
[51] S. Yan, M. Sorrell, Z. Berman, Functional interplay between ATM/ATR-mediated DNA damage response and DNA repair pathways in oxidative stress, Cell Mol. Life Sci. 71 (20) (2014) 3951–3967.
[52] J. Nakamura, D.K. La, J.A. Swenberg, 5′-nicked apurinic/apyrimidinic sites are resistant to beta-elimination by beta-polymerase and are persistent in human cultured cells after oxidative stress, J. Biol. Chem. 275 (858) (2000) 5323–5328.
[53] M. Dizdaroglu, P. Jaruga, M. Birincioglu, H. Rodriguez, Free radical-induced damage to DNA: mechanisms and measurement, Free Radic. Biol. Med. 32 (11) (2002) 1102–1115.
[54] M. Simonatto, L. Latella, P.L. Puri, DNA damage and cellular differentiation: more questions than responses, J. Cell Physiol. 213 (3) (2007) 642–648.
[55] P.L. Puri, K. Bhakta, L.D. Wood, A. Costanzo, J. Zhu, J.Y. Wang, A myogenic differentiation checkpoint activated by genotoxic stress, Nat. Genet 32 (4) (2002) 585–593.
[56] R. de Senzi Moraes Pinto, R. Ferretti, L.H. Moraes, H.S. Neto, M.J. Marques, E. Minatel, N-acetylcysteine treatment reduces TNF-alpha levels and myonecrosis in diaphragm muscle of mdx mice, Clin. Nutr. 32 (3) (2013) 472–475.
[57] J.R. Terrill, H.G. Radley-Crabb, M.D. Grounds, P.G. Arthur, N-Acetylcysteine treatment of dystrophic mdx mice results in protein thiol modifications and inhibition of exercise induced myofibre necrosis, Neuromuscul. Disord. 22 (5) (2012) 427–434.
[58] I.M. Ward, J. Chen, Histone H2AX is phosphorylated in an ATR-dependent manner in response to replicational stress, J. Biol. Chem. 276 (51) (2001) 47759–47762.
[59] K. Malathi, Y. Xiao, A.P. Mitchell, Catalytic roles of yeast GSK3beta/shaggy homolog Rim11p in meiotic activation, Genetics 153 (3) (1999) 1145–1152.
[60] P. Chomczynski, N. Sacchi, The single-step method of RNA isolation by acid guanidinium thiocyanate-phenol-chloroform extraction: twenty-something years on, Nat. Protoc. 1 (2) (2006) 581–585.
[61] G. Smyth, Limma: linear models for microarray data, in: V.C.R. Gentleman, S. Dudoit, W. Hubert (Eds.), Bioinformatics and Computational Biology Solutions unsing R and Bioconductor, Springer, New York, 2005, pp. 397–420.
[62] S.J. Wiklund, E. Agurell, Aspects of design and statistical analysis in the Comet assay, Mutagenesis 18 (2) (2003) 167–175.